


EXPRESS LETTER

Open Access



Monitoring volcanic activity with distributed acoustic sensing using the Tongan seafloor telecommunications cable

Masaru Nakano^{1*} , Mie Ichihara², Daisuke Suetsugu¹, Takao Ohminato², Shigeaki Ono¹, Rennie Vaiomounga³, Taaniela Kula³ and Masanao Shinohara²

Abstract

The devastation caused by the January 2022 eruption of Hunga Tonga-Hunga Ha'apai volcano (HTHH) in the Tongan archipelago reminded us of the importance of monitoring shallow-sea volcanic activity. Seismic observations are essential for such monitoring, but there were no operational seismic stations in Tonga at the time of the eruption. There are only a few islands near Tongan volcanoes, and installation and maintenance of seismic stations on remote islands are expensive. Seismic observations based on distributed acoustic sensing (DAS) using a seafloor cable may provide a more practical and economical solution. To investigate the potential of this approach, we made preliminary DAS observations for 1 week using the seafloor domestic broadband telecommunications cable in Tonga. DAS equipment was installed at the landing station of the seafloor cable at Nuku'alofa on Tongatapu, the main island of Tonga. To provide reference data, we installed several seismometers on Tongatapu. The DAS data we obtained showed high noise levels in areas of shallow coral reef, but noise levels decreased greatly in deeper water areas, indicating that DAS is suitable for seismic observations of the deep seafloor. We detected many local and regional earthquakes during our week of observation and determined 17 earthquake hypocenters by picking P- and S-wave arrival times from the DAS and onshore seismic data. Although most of these were tectonic events related to the subduction of the Pacific plate along the Tonga trench, several events were detected around the volcanic chain of the Tongan archipelago including one event beneath the HTHH crater, implying that activity at HTHH has continued since the 2022 eruption. The much lower cost of installation of DAS equipment compared to that for pop-up type ocean-bottom seismometers and the ability of DAS systems to monitor seismic activity in real-time make it an attractive option for monitoring the activity of HTHH and other volcanoes near seafloor cables in the Tongan archipelago.

Keywords Distributed acoustic sensing, Volcano monitoring, Ocean-floor seismic observations

*Correspondence:

Masaru Nakano

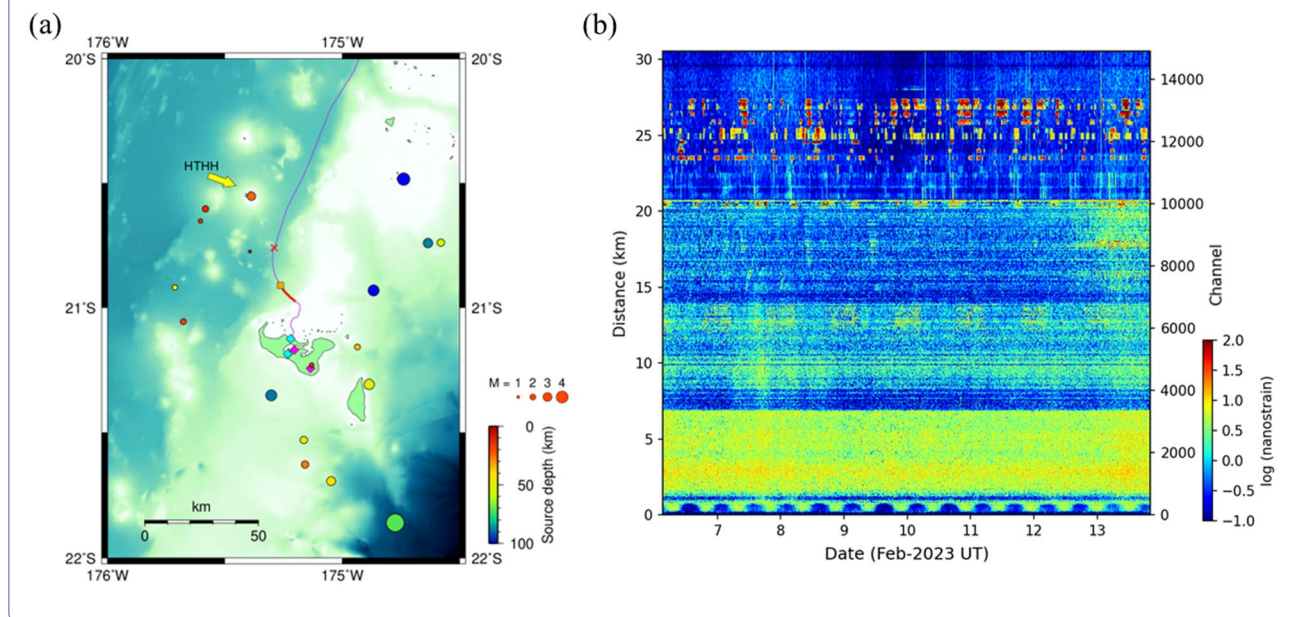
mnakano@jamstec.go.jp

Full list of author information is available at the end of the article



© The Author(s) 2024. **Open Access** This article is licensed under a Creative Commons Attribution 4.0 International License, which permits use, sharing, adaptation, distribution and reproduction in any medium or format, as long as you give appropriate credit to the original author(s) and the source, provide a link to the Creative Commons licence, and indicate if changes were made. The images or other third party material in this article are included in the article's Creative Commons licence, unless indicated otherwise in a credit line to the material. If material is not included in the article's Creative Commons licence and your intended use is not permitted by statutory regulation or exceeds the permitted use, you will need to obtain permission directly from the copyright holder. To view a copy of this licence, visit <http://creativecommons.org/licenses/by/4.0/>.

Graphical Abstract



Main text

Introduction

The devastation caused by the eruption of the Hunga Tonga-Hunga Ha'apai volcano (HTHH) on 15 January 2022 reminded us of the importance of monitoring shallow-sea volcanoes. This eruption radiated strong atmospheric pressure waves as well as seismic waves that were observed worldwide (e.g., Matoza et al. 2022; Wright et al. 2022; Yuen et al. 2022; Garza-Girón et al. 2023). A volcanic explosivity index of about 6 has been estimated based on far-field seismic waves (Poli and Shapiro 2022) and atmospheric waves (Lamb waves) recorded worldwide (Yuen et al. 2022). Yuen et al. (2022) also compared the umbrella cloud radius, lightning, and the initial seismic event magnitude with VEIs of other large eruptions to support their estimation. Among the multidisciplinary approaches used to analyze the eruption, seismological analyses based on global data sets have made the most significant contribution to our understanding of the HTHH eruption. Modeling of the source process of the strong seismic waves radiated by the main eruption has shown that the seismic signals of the eruption consisted of four distinct pulses, for which the waveforms were coherent worldwide and exhibited polarities that were consistent over the full range of azimuths (Poli and Shapiro 2022; Thurin et al. 2022; Yuen et al. 2022; Garza-Girón et al. 2023; Tarumi and Yoshizawa 2023; Zheng et al. 2023). These results imply that the source mechanism for each pulse was a vertical single force, an isotropic source,

a compensated linear vector dipole, or combinations of these mechanisms, although the exact mechanism of the eruption remains debated (e.g., Thurin et al. 2022; Garza-Girón et al. 2023; Zheng et al. 2023).

Detailed analyses by Kintner et al. (2023) of the global seismic data related to the HTHH eruption in 2022 showed that several Mw 4.5 events occurred immediately before the eruption, that strong seismicity continued for 1 week after the eruption, and that the detected seismicity continued for several months. These earthquakes were located at depths of about 10 km in an area of about 25 km² some 10 km southwest of the main HTHH crater.

Data recorded closer to the volcano would likely have revealed precursory activities in more detail, but no seismic stations were operational near HTHH at the time of the eruption (Garza-Girón et al. 2023; Kintner et al. 2023). In response to the HTHH eruption, inactive seismic stations have been returned to operational status and new stations deployed in the Tongan archipelago (Additional file 1: Fig. S1; Government of Tonga, Geoscience Australia, and GNS Science 2022). Although this expanded seismic network has greatly improved volcanic monitoring in Tonga, the stations are tens of km far from the volcanoes and their number is still limited because there are only a few islands that are suitable for permanent seismic stations and the high costs of their installation and maintenance.

Seafloor seismic observations near underwater volcanoes will improve our understanding of seismic activities

related to volcanic eruptions (e.g., Sakai et al. 2001; Saurer et al. 2022). Ideally, real-time monitoring using a cabled ocean-bottom seismometer network near volcanoes would satisfy this need, but the cost and logistics of installing suitable cabled ocean-bottom seismic stations in the Tongan archipelago are unrealistic.

Seismic observations based on distributed acoustic sensing (DAS) can solve these issues. DAS is a recently developed method to estimate dynamic strain along a fiber-optic cable and has been applied to seismic observations in which seafloor fiber-optic cables are used to simulate dense arrays of seismometers (e.g., Lindsey et al. 2017, 2019; Jousset et al. 2018; Wang et al. 2018; Sladen et al. 2019; Williams et al. 2019; Zhan 2019; Fukushima et al. 2022). Because the deep ocean floor is free of anthropogenic noise, high-quality seismic data can be obtained by this technology (Ide et al. 2021; Lior et al. 2021; Shinohara et al. 2022), although noise from natural sources as whale voice or oscillations due to ocean-bottom current sometimes contaminate the signals (e.g., McDonald et al. 1995; Mata Flores et al. 2023). DAS applied to monitoring onshore volcanoes as Etna volcano, Italy (Currenti et al. 2021; Jousset et al. 2022), Vulcano, Italy (Currenti et al. 2023), Azuma volcano, Japan (Nishimura et al. 2021), and tectonic slow earthquakes (Baba et al. 2023) has demonstrated the capability to observe a wide range of seismic signals. Because DAS equipment can be installed at the landing stations of fiber optic cables, ocean-floor seismic motions can be recorded in real time with installation and maintenance costs far lower than those of ocean-bottom seismometers or seismic stations on remote islands.

There are both international and domestic fiber-optic seafloor telecommunication cable systems in Tonga. The international cable connects Tongatapu, the main island of the Tongan archipelago, to Fiji, whereas the domestic cables run along the volcanic archipelago, connecting Tongatapu to Vava'u and Ha'apai islands (see Fig. 1). Both cable systems were disrupted by the 2022 HTHH eruption (Clare et al. 2023). The international cable was repaired within a month of the eruption, but it took more than a year to repair the domestic cable system. During the eruption, the domestic system was disrupted about 47 km north along the cable from the landing station on Tongatapu, and later cut 31 km from the landing station during repair operations (Fig. 1). Accordingly, the cable was missing between 31 and 100 km from Tongatapu (Tonga Cable Ltd. 2022; Clare et al. 2023).

In this study, we carried out DAS experiments using the Tongan domestic seafloor fiber-optic telecommunication cable to assess the feasibility of DAS to monitor volcanic activity in the Tongan archipelago. DAS data are normally acquired using a dark fiber (i.e., one that

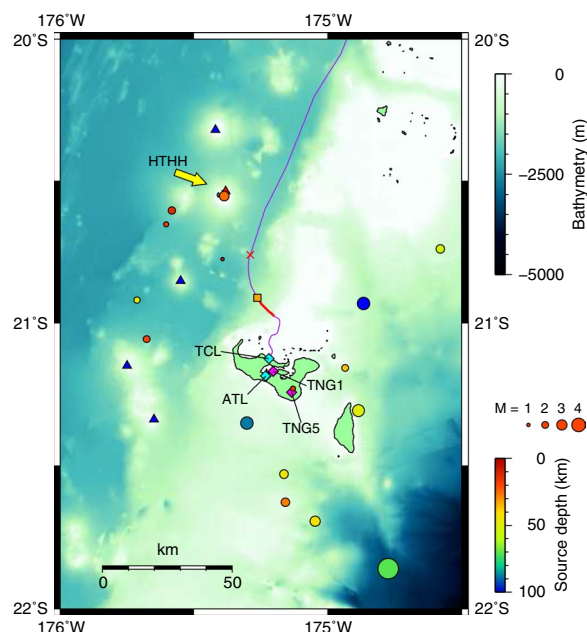


Fig. 1 Regional map showing the domestic seafloor cable route and the hypocenter distribution around Tonga. The purple line indicates the cable route; the section of cable used for hypocenter determinations from DAS data is shown in red. The red cross indicates the location where the cable was cut by the 2022 HTHH eruption and the orange square indicates where the cable was cut during post-eruption repair operations. Circles indicate hypocenters obtained from DAS observations in this study. The light blue and pink diamonds are locations of temporary and permanent onshore seismic stations, respectively. Red and blue triangles are onshore and ocean-bottom volcanoes, respectively (Global Volcanism Program 2023). The yellow arrow indicates the location of HTHH volcano. Bathymetry is from the ETOPO Global Relief Model (NOAA 2022)

carries no other signals), but neither the international nor the domestic Tongan cables have unused fibers. Consequently, DAS observations using those cables would be difficult during periods of telecommunication operations. However, Tonga Cable Ltd. (TCL) allowed us to use the domestic cable for our DAS experiments in February 2023, before repairs were completed. In addition, we installed seismometers at two sites on Tongatapu. Our DAS data detected many local and regional earthquakes as small as local magnitude 1, demonstrating that DAS can be a powerful tool for monitoring submarine volcanic activity in real time.

Observations

We conducted our seismic observations in Tonga between 6 and 13 February 2023. For the DAS observations, we used the domestic cable. We installed a DAS interrogator on Tongatapu to record ground oscillations along the 31-km segment of cable extending

north from the landing station to the southern end of the damaged section, which lies about 40 km south-southeast from the center of HTHH (Fig. 1). We used an OptaSense QuantX DAS interrogator for the DAS observations. In DAS systems, the phase shift between the gauge length is used to estimate the fiber strain, which measurement is conducted at every channel interval along the fiber at the pulse rate in time. We set the gauge length at 30.63 m, channel interval at 2.042 m (14,960 channels), pulse rate at 3.125 kHz, and strain waveforms were recorded at 312.5 Hz after decimation.

We also installed two seismic stations on Tongatapu, one at the TCL facility and the other at an electromagnetic station about 7 km inland from the TCL facility. At each station, we installed a pair of seismometers: a Nanometrics Trillium Compact (120 s period) and a Lenartz LE-3Dlite MKIII (1 s period). Data were sampled at 200 Hz and recorded by a Hakusan LS8800 data logger (24-bit, differential input ± 5 V). We also used data recorded during our study period by the Tongan archipelago seismic network (Government of Tonga, Geoscience Australia, and GNS Science 2022) (Additional file 1: Fig. S1).

DAS records obtained during the entire observation period are shown in Fig. 2. Between about 23 and 27 km from the landing station, there are several series of dramatic increases of strain amplitude that lasted over periods of tens of minutes to hours over particular stretches of cable up to several hundred meters long. The occurrence time of these phenomena seems generally irregular, but correlates spatially for some segments. Although the cause of this behavior is unclear, it may reflect cable oscillations due to intermittent bottom currents (e.g., Williams et al. 2022; Mata Flores et al. 2023). Sounds from ship screw or whale voice (McDonald et al. 1995; Ugalde et al. 2021) cannot explain the long durations of the oscillations at fixed cable segments.

Records of local and regional earthquakes detected during our study period (Fig. 3) clearly show P- and S-wave arrivals along the cable, even for the observations of horizontal strain on the seafloor (e.g., Ide et al. 2021; Lior et al. 2021).

Earthquake hypocenter determinations

We observed many regional and local earthquake signals during our study (Fig. 3). We determined the hypocenter locations by using both the DAS data and the

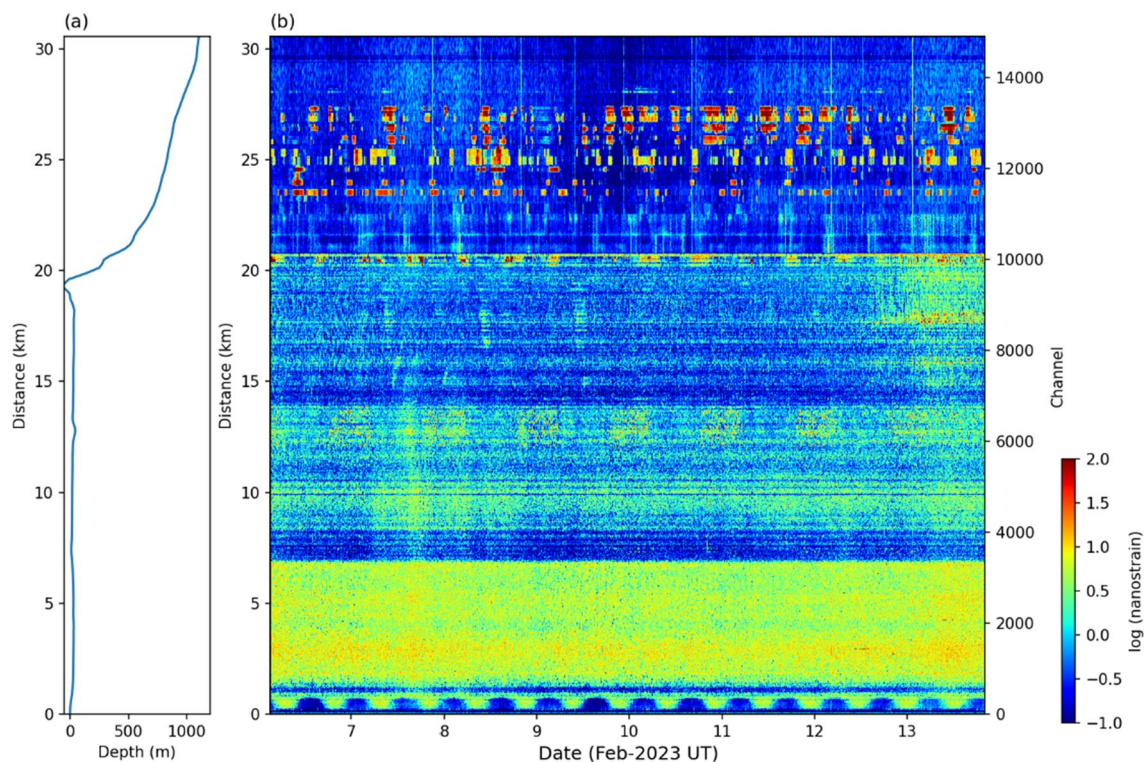


Fig. 2 Cable depth and DAS records for the entire observation period. **a** Seafloor depth along the cable route was derived from the ETOPO Global Relief Model (NOAA 2022). **b** DAS records plotted against length of cable from the landing station at Nuku'alofa, Tonga. DAS strain waveforms were band-pass filtered between 1 and 20 Hz and their absolute amplitudes are plotted at log scale

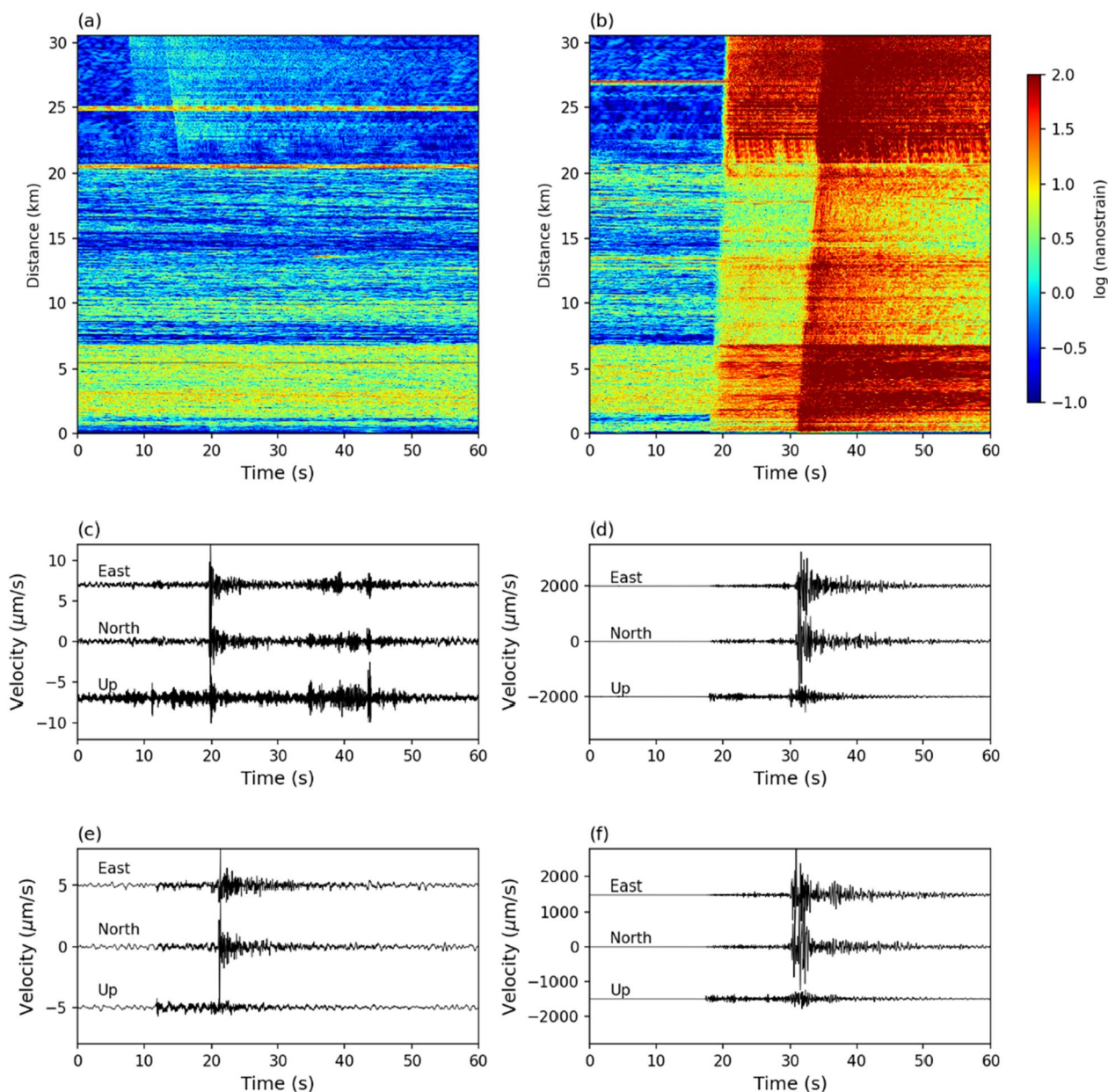


Fig. 3 Examples of earthquake records obtained by DAS and onshore seismic stations. **a, c, e** A magnitude 2.8 earthquake beneath the HTHH crater at 07:40:55 (UT) on 12 Feb. 2023. **b, d, f** The largest earthquake (magnitude 6.1) recorded during the observation period at 01:21:42 (UT) on 13 Feb. 2023. **a, b** are DAS strain records. **c, d** are ground velocities recorded by Nanometrics Trillium Compact seismometers at the TCL station. **e, f** are ground velocities at station TNG1. The x-axes show elapsed time from the event origin. Strain and velocity seismograms were band-pass filtered between 1 and 20 Hz. Earthquake magnitudes are those estimated in this study

onshore seismometer records. We applied the STA/LTA event trigger (e.g., Allen 1978; Withers et al. 1998) to the DAS records after 1–20 Hz band-pass filtering, which we set the STA and LTA window lengths at 3 and 24 s, respectively. We used DAS traces from every 100th channel (effectively a 204 m interval) between channels 13,500 and 14,900 (i.e., channels 13,500,

13,600, ..., 14,900), thereby avoiding the segments that showed the intermittent high noise levels described in the previous section. We then applied the network coincidence trigger of Trnkoczy (2012) with the coincidence sum threshold set at 5 channels by using the ObsPy toolbox for seismology (Beyreuther et al. 2010). The detected events were then visually inspected to

identify and remove false triggers. We detected more than 160 events.

We then manually picked P- and S-wave arrival times for DAS traces from every 100th channel (i.e., channels 11,000, 11,100, ..., 14,900). We selected events with clear P- and S-wave onsets for channels between 14,000 and 14,900 from the DAS records with S – P onset time differences of less than ~ 15 s at channel 14,900. We chose this criterion to evaluate the seismic monitoring capability of DAS around HTHH for data recorded near the end of the cable. We also picked first motions from seismic records obtained at our temporary onshore seismometers and those from permanent stations in and around Tonga that we downloaded from the Incorporated Research Institutions for Seismology Data Management Center (IRIS-DMC) website. We used the P-wave crustal velocity structure obtained by a seismic survey over the Tonga ridge (Crawford et al. 2003) and assumed $V_p/V_s=1.73$, where V_p and V_s are P- and S-wave velocities, respectively. Hypocenters were obtained using the method of Hirata and Matsu'ura (1987), which estimates the hypocenter location based on the maximum-likelihood method, and earthquake magnitudes were estimated from the peak velocity obtained at onshore stations by using the empirical formula of Watanabe (1971, Additional file 1: Text S1).

We determined hypocenters for 17 events with magnitudes of 1.0–6.1 that occurred during our study period at depths of 8–106 km (Fig. 1, Additional file 2). Errors of the epicenter locations are shown in Additional file 1: Fig. S2 and depth error was about 10 km. Only the largest event was of sufficient magnitude to be included in the U.S. Geological Survey (USGS) earthquake catalog. Although most of the earthquakes we recorded were tectonic events related to the subduction of the Pacific plate along the Tonga trench, several events were detected around the volcanic chain of the Tongan archipelago including one event directly beneath the HTHH crater (Fig. 1). Earthquake activity beneath HTHH has previously been attributed to the HTHH eruption (Kintner et al. 2023). Our detection of an event beneath the volcano suggests that HTHH was still seismically active during our study period.

We next considered the event detection limit around HTHH based on the DAS data acquired using the domestic seafloor cable. Figure 4 shows the earthquake magnitudes we determined plotted against the epicentral distance from channel 14,900 (i.e., the northern end of the available section of the cable). Because the distance from HTHH to the nearest point on the domestic cable route is about 20 km (Fig. 1) and because a DAS cable effectively constitutes a dense linear array of seismometers, earthquakes as small as magnitude 1 beneath

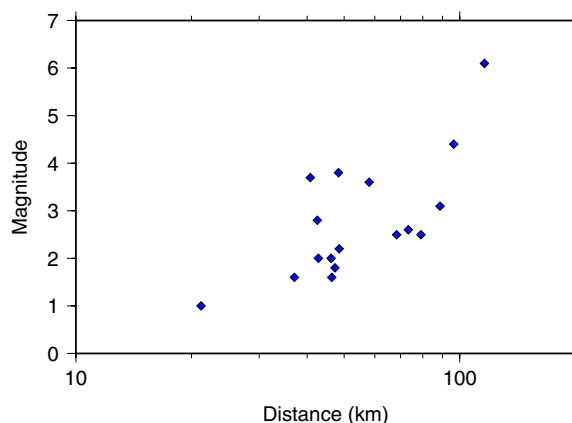


Fig. 4 Earthquake magnitudes plotted against epicentral distance

HTHH would be detectable by DAS if we could use the segment of cable beyond 31 km from the landing station (i.e., north of channel 14,900), which was missing during our observation period. Since DAS measures seismic signals at intervals of several to tens of meters, signals from small events are recorded by sufficient channels to allow us to distinguish signal from noise.

Ambient noise levels

Although ambient noise levels were generally high along the first 21 km of cable north of the landing station, where water depths are less than 10 m with areas of coral reef (Fig. 2), they then decreased rapidly as water depth increased northward to about 1000 m. In the area of shallow reefs along the first 7 km of cable, noise levels were several times higher than along the segment from 7 to 21 km, even though water depths there were similar. The amplitudes of earthquake signals detected show similar trends with noise levels between 0 and 21 km segment (Fig. 3 and Additional file 1: Fig S3). These observations imply that the differences in noise levels do not reflect differences in the actual levels of ambient noise; rather, they represent differences in amplification factors due to soft surface soil or weak cable–seafloor coupling. Because the earthquake signal amplitudes recorded along the 7–21 km cable segment were much lower than those from the cable in deeper water beyond 21 km, we consider that the cable–seafloor coupling was relatively weak along the 7–21 km cable segment.

We computed power spectral density (PSD) hourly for channels 2000, 8000, and 14,000 during our entire observation period (Fig. 5), and Additional file 1: Fig. S4 provides the probability density functions of PSDs computed for other channels (McNamara and Buland 2004). PSDs plotted against cable length for selected frequencies show that noise levels between channels

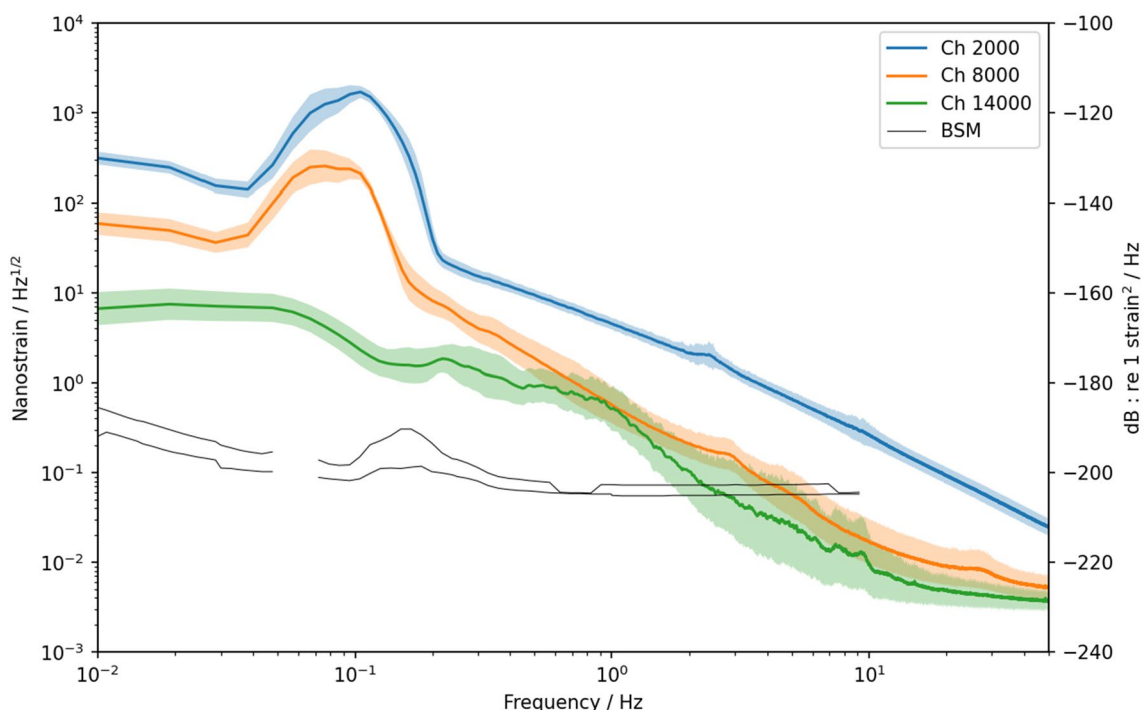


Fig. 5 Power spectral densities of DAS records at channels 2000 (4.08 km from landing station), 8000 (16.32 km), and 14,000 (28.56 km) over the duration of our study. Lines and shaded areas indicate the average and standard deviation, respectively. The standard deviation of borehole strain-meter (BSM) data measured onshore in southern California in 2009 (black lines) are shown for comparison (Barbour and Agnew 2011)

11,500 and 13,400 showed larger standard deviation compared with other channels (Additional file 1: Fig. S5) and the PSD at channel 12,000 was bimodal (Additional file 1: Fig. S4e), which we attribute to intermittent increases in strain amplitude (Fig. 2). These data highlight the considerably different noise levels for channels 0–3400 (0–7 km) and 3400–10,200 (7–21 km), which are also evident in Fig. 2.

Noise levels were generally high at lower frequencies, but decreased considerably at higher frequencies for all channels (Fig. 5 and Additional file 1: Fig S4), similar to observations acquired using a seafloor cable deployed off Kamaishi, northeast Japan (Shinohara et al. 2022). The PSDs commonly show several peaks below 2 Hz. The power of the primary mode of microseisms was high at around 0.04–0.2 Hz (5–25 s) for channels on the shallow seafloor (< 21 km from the landing station); this peak has been attributed to the passing of ocean waves in shallow water (e.g., Cessaro 1994; Arduin et al. 2015) and has a considerable effect on channels in the areas of coral reefs in our study. In contrast, the secondary mode of microseisms appears between 0.1–2 Hz (0.5–10 s) for channels in deeper water. This mode has been attributed to the action of oceanic waves in coastal and pelagic regions and is dominant for cable segments in the deeper water (Cessaro 1994; Nishida 2017).

Compared with onshore borehole strain-meter (BSM) data recorded in southern California (Barbour and Agnew 2011), the seafloor noise levels of our DAS observations are higher at frequencies below 2 Hz, even in regions of deep water (Fig. 5). This feature may be inherent to the DAS interrogators themselves (Shinohara et al. 2022). In contrast, the noise levels at greater than 1 Hz are comparable with, or lower than, those of BSM data for cable segments in deeper water and are similar to those obtained at Kamioka, central Japan, which is one of the quietest sites in the world (Araya et al. 2017). Although the cable coupling ratio with the seafloor is not well known, the noise levels obtained in this study were similar to those obtained by Shinohara et al. (2022) in deep water off Kamaishi. These observations indicate that ambient noise levels in deep water are very low and DAS observations under these conditions are suitable for monitoring seismic activities around the volcanoes in the Tongan archipelago.

We computed a running spectrum for a 1-day record (8 February 2023) at channel 12,000 (Additional file 1: Fig. S6) during the period of intermittent increases of strain amplitude. During strong oscillation, noise levels increased at around 0.5 Hz and several higher modes were evident. The peak frequency increased slightly during the oscillation, then recovered to the starting

frequency when the oscillation ceased. The strain records are generally similar among the channels during the oscillation. We consider that the oscillation of the cable segment was caused by bottom currents (e.g., Williams et al. 2022). Ide et al. (2021) reported periodic cable strain changes of >20 micro-strains due to diurnal and semidiurnal tides. Although the periodicity of the strong oscillation in our records is not clear, ocean tides may have caused bottom currents and the resultant cable oscillations (Mata Flores et al. 2023).

Discussion

For our hypocenter determinations, we determined earthquake magnitudes based on records from onshore seismometers. However, if the signals for small events were recorded only by DAS, we need to determine earthquake magnitudes from only DAS strain records. We therefore attempted to estimate event magnitudes based on our DAS data alone, which may be a helpful approach for small events at HTHH that are detected only by proximal DAS channels. In this approach, we considered only the cable-end channels. We estimated the epicentral distance empirically from the arrival time difference of the P- and S-waves ($S-P$) according to the Omori formula, then obtained the earthquake magnitude from the maximum strain amplitudes of the channels corrected for the site amplification and cable–seafloor coupling. Assuming a plane wave, DAS strain records can be converted to velocity records by multiplying them by the apparent velocity (V_{app}) of the incident waves along the cable (e.g., Wang et al. 2018). In this way, event magnitudes are roughly estimated from the maximum velocity computed from the DAS strain amplitudes.

This approach uses some empirical parameters, such as V_p , V_s , and site factor that includes the effects of the site amplification and cable–seafloor coupling. We empirically estimated V_p , V_s , and the site factor from earthquakes for which hypocenters were determined in this study and for which P- and S-waves were clearly recognized in the DAS records at the cable-end channels. We first estimated the P-wave velocity by assuming $V_p/V_s=1.73$. From the $S-P$ times picked at channel 14,900 and the hypocentral distance, we obtained the average $V_p=5.4$ km/s from the Omori formula (Additional file 1: Fig. S7). This value roughly corresponds to the P-wave velocity obtained at about 4 km depth by Crawford et al. (2003). Then we computed the average maximum strain after S-wave arrivals at every 100th channel between 14,000 and 14,900 because DAS strain amplitudes strongly vary even in this narrow range, probably due to heterogeneities in the shallow crust and differences in cable–seafloor coupling. We also estimated the apparent velocity of seismic signal from the S-wave

arrival time difference between channels 14,000 and 14,900. We then obtained the maximum velocity at the cable end from the maximum strain multiplied by the apparent velocity. Then, we estimated the site factor from the maximum velocity divided by that expected from the formula of Watanabe (1971). The site factor was 8.0 in average at logarithmic scale (Additional file 1: Fig. S8). We compared event magnitudes estimated by the empirical method with those from the hypocenter determinations (Additional file 1: Fig. S9). The empirical method well reproduced the observed event magnitudes. This method could provide early estimations of activities around HTHH in addition to back azimuth estimations from travel times along the cable. This method can be easily automated if we pick P- and S-wave onsets automatically. Although rough estimations of arrival times based on STA/LTA may work, more precise picks based on machine learning methods (e.g., Zhu and Beroza 2019) applied to the seafloor DAS strain records may provide better estimations. In the empirical estimations of event magnitude, relatively large positive and negative deviations from local magnitude could be found for signals coming from the directions parallel to (147 and 327°) and perpendicular to (57 and 237°) the cable alignment, respectively (Additional file 1: Fig. S10). These results imply that the fiber strain responses depend on the incident angles of the seismic signals (e.g., Zhan 2019), but more event data are necessary for further investigations.

With real-time DAS observations using the seafloor cable, we can continuously monitor the seismic activities around HTHH and the volcanoes in the Tongan archipelago. Various types of seismic events occur around volcanoes including volcano tectonic (VT), long-period (LP), and very-long-period (VLP) events and volcanic tremor (e.g., Chouet 1996, 2003; Konstantinou 2023) which are used to monitor volcanic activities (e.g., Umakoshi et al. 2001; Yukutake et al. 2019). Currenti et al. (2023) detected signals from LP and VLP events using DAS technology applied to land and seafloor fiber-optic cables located within 10 km from the summit crater at Vulcano. VT events share the waveform characteristics with ordinary earthquakes and the detection limit was magnitude about 1 by our DAS observation (Fig. 4). Although earthquakes related to volcanic activities are small in many cases, those with magnitude larger than 1 were observed during an activity without significant eruptions at Hakone volcano, Japan (Yukutake et al. 2011). LP events and volcanic tremor are dominated in signals between 0.5 and 5 Hz (e.g., Chouet et al. 1994; Chouet 1996; Konstantinou and Schlindwein 2003; Chouet and Matoza 2013). Noise levels of this band were several times larger than those of higher frequency components in our DAS experiment (Fig. 5) and the detection limit would be slightly larger

than VT events. Detections of VLP events, dominated in signals with several tens of seconds, would be challenging because the DAS noise levels was more than 100 times larger in this frequency band than higher frequency components. However, Ohminato et al. (1998) detected VLP events of moment magnitude about 3 at Kilauea volcano. Since this size of earthquakes radiate seismic waves 1000 times larger than those of magnitude 1, larger VLP events could be detected by DAS in Tonga. We tried to detect LP and VLP events from our DAS data in Tonga. After band-pass filtering the strain records between 0.1 and 5 Hz for LP events and between 0.01 and 0.1 Hz for VLP events, we applied the STA/LTA event trigger for each dataset. However, we did not detect any distinct signals from these types of events.

During our observation period, two events that occurred about 100 km south-southeast of Tongatapu were added to the USGS earthquake catalog (Additional file 1: Table S1). Both events were detected by our DAS, but the hypocenter of one of them was not determined because the S-wave onsets were disturbed by overlapping strong P-wave coda, probably because of the shallow source depth. We determined the hypocenter of the other event to be about 80 km northeast of that recorded in the USGS catalog. We attribute this error to the fact that the event occurred outside the observation network we used. The magnitude we calculated for this event was 1.4 magnitude scale larger than that in the USGS catalog. Because our magnitude determination was based on seismometer records obtained in the Tongan archipelago, the signals were strongly amplified by the soft surface layers of corals; the USGS did not use data from stations in the Tongan archipelago, so such signal amplification was not an issue in their determination. If all of our event magnitudes were overestimated, the event detection limit we used should be lower. Calibrations using more events are necessary to obtain more accurate magnitudes.

Kintner et al. (2023) obtained precise hypocenter distributions relative to the main seismic event of the 2022 HTHH eruption. Earthquakes of magnitude larger than 3.9 were distributed within an area 5–10 km southwest of the summit crater. Our DAS observations detected an event of magnitude 2.8 beneath HTHH, close to the active area obtained by Kintner et al. (2023). We consider this event to be indicative of ongoing activity at HTHH, but because this was the only event we detected during our week of observation, that activity may be intermittent. DAS observations will be a powerful tool for real-time monitoring of any future activity at HTHH. Future automation of hypocenter determinations based on amplitude distributions and travel-time differences between adjacent DAS channels (Nishimura et al. 2021) would further improve the monitoring capability.

By using DAS technology, we recorded real-time seismic activity at the seafloor close to HTHH. The installation of DAS equipment at the landing station of the Tongan domestic telecommunications cable took only a few hours, thus demonstrating that this technology can be rapidly deployed in emergency situations at other sites where fiber-optic cables are near volcanoes. Unfortunately, because there are no dark fibers in the Tongan seafloor cables, and the both the international and domestic cables are in operational state now, future monitoring of Tongan volcanoes requires the development of DAS equipment that uses a laser with a wavelength that does not interfere with telecommunication signals. This might be achieved by using wavelength division multiplexing technology.

Conclusions

We carried out distributed acoustic sensing (DAS) observations close to the HTHH volcano by using the Tongan domestic fiber-optic seafloor telecommunications cable for 1 week about 1 year after the devastating January 2022 HTHH eruptions. We detected many regional and local earthquakes including one beneath the HTHH crater, thus demonstrating that DAS observations can be a powerful tool for real-time volcanic monitoring. Because the cable runs along the volcanic chain of the Tongan archipelago, DAS can also be used to monitor activity at other volcanoes in the chain. The maintenance costs for DAS systems are low because the equipment can be installed at cable landing stations.

The Tongan seafloor cables do not have dark fibers to put DAS signals. By making use of the unused cable in the period before the repair of damage due to the 2022 eruption of HTHH, we obtained a precious dataset that allowed us to examine the feasibility of DAS observations to monitor the activity of oceanic and island volcanoes. Our results demonstrate that the development of DAS equipment that does not interfere with telecommunication signals and allows regular real-time volcanic monitoring is well worthwhile.

Abbreviations

HTHH	Hunga Tonga-Hunga Ha'apai volcano
DAS	Distributed acoustic sensing
TCL	Tonga Cable Ltd.
IRIS-DMC	Incorporated Research Institutions for Seismology Data Management Center
USGS	U.S. Geological Survey
PSD	Power spectral density
BSM	Borehole strain meter
VT	Volcano tectonic
LP	Long-period
VLP	Very-long-period

Supplementary Information

The online version contains supplementary material available at <https://doi.org/10.1186/s40623-024-01972-2>.

Additional file 1: Fig S1. Regional map showing the seismic stations and volcanoes around Tonga. Diamonds show the permanent seismic stations installed after the HTHH eruption. The pink diamonds are the stations used in this study. The red and blue triangles mark land and ocean-bottom volcanoes, respectively (Global Volcanism Program 2023). **Fig S2.** Map showing errors of hypocenter determinations. Error ellipsoids are plotted at each epicenter (white circles). Purple and red lines and diamonds are the same as in Fig. 1. **Fig S3.** Comparison of amplitudes during an earthquake and background noise. Orange line represents the maximum amplitude during the event shown in Fig. 3b. Blue line indicates average amplitudes between 0 and 10 sec in Fig. 3b, before the P-wave arrival of the event. **Fig S4.** The probability density functions of ambient noise spectra of DAS strain records at selected channels. The blue lines and shaded areas indicate the average and standard deviation during the observation period, respectively. Orange lines are hourly computed PSDs. **Fig S5.** PSDs of DAS strain records for selected frequencies plotted against channel number. Lines and shaded areas indicate averages and standard deviations during the observation period, respectively. **Fig S6.** Running spectrum for 1 day of recording at channel 12,000. **Fig S7.** $S - P$ time versus event distance. The blue line is calculated assuming $V_p = 5.4$ km/s and $V_p/V_s = 1.73$ according to the Omori formula. **Fig S8.** Site factor computed from maximum velocity of seismic motion from DAS observation (V_{max}^{DAS}) and that expected from the event magnitude (V_{max}^{calc}). The blue line is an average value at logarithmic scale. **Fig S9.** Comparison of magnitudes from hypocenter determinations (x-axis) and those estimated using empirical parameters from DAS records (y-axis). **Fig S10.** Difference of magnitude empirically estimated from DAS records and local magnitude plotted against the back azimuth. **Table S1.** Events around Tonga obtained from the USGS earthquake catalog.

Additional file 2: Event list obtained in this study.

Acknowledgements

We are grateful to the Tonga Cable Ltd. for permissions to use the domestic fiber optic cables and much support during our DAS experiment. We thank Mr. T. Yagi (ERI), V. Tovi (TGS), and members of Tonga Geological Services for their assistance. We are grateful to Dr. A. Lemarchand (IPGP) for helpful comments to the experimental design. Several figures were drawn using Generic Mapping Tools (Wessel and Smith 1998). We thank three anonymous reviewers and the editor K. Konstantinou for careful review and constructive comments, which have improved the manuscript.

Author contributions

MN performed the data processing and analyses. MI initiated the study. MN, MI, MS, and TO carried out DAS and field seismic observations. MN, MI, TO, DS, and RV designed the observation plan. MI, TO, TK, RV, and SO organized the observations in Tonga. All authors read and approved the final manuscript.

Funding

This study is funded by ERI of the University of Tokyo and JAMSTEC with the support of Tonga Geological Services (TGS), Tonga Cable Ltd., and Japan International Cooperation Agency (JICA). This study was also supported by JSPS KAKENHI Grant Number 22H00251 (to SO) and Japan Science and Technology Agency (JST) through Science and Technology Research Partnership for Sustainable Development (SATREPS) project ID 23727132 (to MI).

Availability of data and materials

Records from our DAS and temporary onshore seismic station observations are available from the authors on reasonable request. Event list obtained in this study is available from Additional file 2. Data from permanent seismic stations in and around Tonga are available from IRIS-DMC (iris.edu). Bathymetry was derived from the ETOPO Global Relief Model (NOAA 2022). Locations of volcanoes around Tonga are available from the website of Global Volcanism Program (2023) (<https://volcano.si.edu/>). USGS NEIC earthquake catalog is available from <https://earthquake.usgs.gov/earthquakes>.

Declarations

Ethics approval and consent to participate

Not applicable.

Consent for publication

Not applicable.

Competing interests

The authors declare no competing interests associated with this manuscript.

Author details

¹Institute for Marine Geodynamics (IMG), Japan Agency for Marine-Earth Science and Technology, 2-15, Natsushima-cho, Yokosuka, Kanagawa 237-0061, Japan. ²Earthquake Research Institute, University of Tokyo, Tokyo 113-0032, Japan. ³Tonga Geological Services, Government of Tonga, 51 Vaha'akolo Road, Nuku'alofa, Tonga.

Received: 12 September 2023 Accepted: 24 January 2024

Published online: 04 February 2024

References

- Allen RV (1978) Automatic earthquake recognition and timing from single traces. *Bull Seism Soc Am* 68:1521–1532
- Araya A, Takamori A, Morii W, Miyo K, Ohashi M, Hayama K, Uchiyama T, Miyoki S, Saito Y (2017) Design and operation of a 1500-m laser strainmeter installed at an underground site in Kamioka, Japan. *Earth Planet Space* 69:77. <https://doi.org/10.1186/s40623-017-0660-0>
- Ardhuin F, Gualtieri L, Stutzmann E (2015) How ocean waves rock the Earth: two mechanisms explain microseisms with periods 3 to 300 s. *Geophys Res Lett* 42:765–772. <https://doi.org/10.1002/2014GL026782>
- Baba S, Araki E, Yamamoto Y, Hori T, Fujie G, Nakamura Y et al (2023) Observation of shallow slow earthquakes by distributed acoustic sensing using offshore fiber-optic cable in the Nankai Trough, southwest Japan. *Geophys Res Lett*. <https://doi.org/10.1029/2022GL102678>
- Barbour AJ, Agnew DC (2011) Noise levels on plate boundary observatory borehole strainmeters in Southern California. *Bull Seism Soc Am* 101:2453–2466. <https://doi.org/10.1785/0120110062>
- Beyreuther M, Barsch R, Krischer L, Megies L, Behr Y, Wassermann J (2010) ObsPy: a python toolbox for seismology. *Seismol Res Lett* 81:530–533. <https://doi.org/10.1785/gssrl.81.3.530>
- Cessaro RK (1994) Sources of primary and secondary microseisms. *Bull Seism Soc Am* 84:142–148
- Chouet BA (1996) Long-period volcano seismicity: its source and use in eruption forecasting. *Nature* 380:309–316
- Chouet B (2003) Volcano seismology. *Pure Appl Geophys* 160:739–788
- Chouet BA, Matoza RS (2013) A multi-decadal view of seismic methods for detecting precursors of magma movement and eruption. *J Volcanol Geotherm Res* 252:108–175. <https://doi.org/10.1016/j.jvolgeores.2012.11.013>
- Chouet BA, Page RA, Stephens CD, Lahr JC, Power JA (1994) Precursory swarms of long-period events at Redoubt Volcano (1989–1990), Alaska: their origin and use as a forecasting tool. *J Volcanol Geotherm Res* 62:95–135
- Clare MA, Yeo IA, Watson S, Wysoczanski R, Seabrook S, Mackay K et al (2023) Fast and destructive density currents created by ocean-entering volcanic eruptions. *Science* 381:6662. <https://doi.org/10.1126/science.adi3038>
- Crawford WC, Hildebrand JA, Dorman LM, Webb SC, Wiens DA (2003) Tonga ridge and Lau Basin crustal structure from seismic refraction data. *J Geophys Res* 108:2195. <https://doi.org/10.1029/2001JB001435>
- Currenti G, Jousset P, Napoli R, Krawczyk C, Weber M (2021) On the comparison of strain measurements from fibre optics with a dense seismometer array at Etna volcano (Italy). *Solid Earth* 12:993–1003. <https://doi.org/10.5194/se-12-993-2021>
- Currenti G, Allegra M, Cannavò F, Jousset P, Prestifilippo M, Napoli R, Sciutto M, Di Grazia G, Privitera E, Palazzo S, Krawczyk C (2023) Distributed dynamic strain sensing of very long period and long period events on telecom fiber-optic cables at Vulcano, Italy. *Sci Rep* 13:4641. <https://doi.org/10.1038/s41598-023-31779-2>

- Fukushima S, Shinohara M, Nishida K, Takeo A, Yamada T, Yomogida K (2022) Detailed S-wave velocity structure of sediment and crust off Sanriku, Japan by a new analysis method for distributed acoustic sensing data using a seafloor cable and seismic interferometry. *Earth Planets Space* 74:92. <https://doi.org/10.1186/s40623-022-01652-z>
- Garza-Girón R, Lay T, Pollitz F, Kanamori H, Rivera L (2023) Solid earth–atmosphere interaction forces during the 15 January 2022 Tonga eruption. *Sci Adv*. <https://doi.org/10.1126/sciadv.add4931>
- Global Volcanism Program (2023) Volcanoes of the world. Smithsonian Institution, Washington, DC. <https://doi.org/10.5479/si.GVPVOTW4-2013>
- Government of Tonga, Geoscience Australia, and GNS Science (2022) Tonga temporary seismic monitoring network. *Int Feder Digit Seismogr Netw*. https://doi.org/10.7914/SN/YC_2022
- Hirata N, Matsu'ura M (1987) Maximum-likelihood estimation of hypocenter with origin time eliminated using nonlinear inversion technique. *Phys Earth Planet Int* 47:50–61
- Ide S, Araki E, Matsumoto H (2021) Very broadband strain-rate measurements along a submarine fiber-optic cable off Cape Muroto, Nankai subduction zone, Japan. *Earth Planet Space* 73:63. <https://doi.org/10.1186/s40623-021-01385-5>
- Jousset P, Reinsch T, Ryberg T, Blanck H, Clarke A, Aghayev R, Hersir GP, Hennings J, Weber M, Krawczyk CM (2018) Dynamic strain determination using fibre-optic cables allows imaging of seismological and structural features. *Nat Comm* 9:2509. <https://doi.org/10.1038/s41467-018-04860-y>
- Jousset P, Currenti G, Schwarz B, Chalari A, Tilmann F, Reinsch T, Zuccarello L, Privitera E, Krawczyk CM (2022) Fibre optic distributed acoustic sensing of volcanic events. *Nat Comm* 13:1753. <https://doi.org/10.1038/s41467-022-29184-w>
- Kintner JA, Yeck WL, Earle PS, Prejean S, Pesicek JD (2023) High-precision characterization of seismicity from the 2022 Hunga Tonga–Hunga Ha'apai Volcanic Eruption. *Seismol Res Lett* 94:589–602. <https://doi.org/10.1785/0220220250>
- Konstantinou KI (2023) A review of the source characteristics and physical mechanisms of very long period (VLP) seismic signals at active volcanoes. *Surv Geophys*. <https://doi.org/10.1007/s10712-023-09800-0>
- Konstantinou KI, Schlindwein V (2003) Nature, wavefield properties and source mechanism of volcanic tremor: a review. *J Volcanol Geotherm Res* 119:161–187. [https://doi.org/10.1016/s0377-0273\(02\)00311-6](https://doi.org/10.1016/s0377-0273(02)00311-6)
- Lindsey NJ, Martin ER, Dreger DS, Freifeld B, Cole S, James SR et al (2017) Fiber-optic network observations of earthquake wavefields. *Geophys Res Lett* 44:11–792. <https://doi.org/10.1002/2017GL075722>
- Lindsey NJ, Dawe TC, Ajo-Franklin JB (2019) Illuminating seafloor faults and ocean dynamics with dark fiber distributed acoustic sensing. *Science* 366:1103–1107. <https://doi.org/10.1126/science.aay5881>
- Lior I, Sladen A, Rivet D, Ampuero JP, Hello Y, Becerril C et al (2021) On the detection capabilities of underwater distributed acoustic sensing. *J Geophys Res*. <https://doi.org/10.1029/2020JB020925>
- Mata Flores D, Sladen A, Ampuero JP, Mercerat ED, Rivet D (2023) Monitoring deep sea currents with seafloor distributed acoustic sensing. *Earth Space Sci*. <https://doi.org/10.1029/2022EA002723>
- Matoza RS, Fee D, Assink JD, Iezzi AM, Green DN, Kim K et al (2022) Atmospheric waves and global seismoacoustic observations of the January 2022 Hunga eruption, Tonga. *Science* 377:6601. <https://doi.org/10.1126/science.abo7063>
- McDonald MA, Hildebrand JA, Webb SC (1995) Blue and fin whales observed on a seafloor array in the Northeast Pacific. *J Acoust Soc Am* 98:712–721. <https://doi.org/10.1121/1.413565>
- McNamara DE, Buland RP (2004) Ambient noise levels in the continental United States. *Bull Seism Soc Am* 94:1517–1527
- Nishida K (2017) Ambient seismic wave field. *Proc Jpn Acad Ser B* 93:423–448. <https://doi.org/10.2183/pjab.93.026>
- Nishimura T, Emoto K, Nakahara H, Miura S, Yamamoto M, Sugimura S, Ishikawa A, Kimura T (2021) Source location of volcanic earthquakes and subsurface characterization using fiber-optic cable and distributed acoustic sensing system. *Sci Rep* 11:6319. <https://doi.org/10.1038/s41598-021-85621-8>
- NOAA (2022) ETOPO 2022 15 arc-second global relief model. NOAA Natl Centres Environ Inform. <https://doi.org/10.25921/fd45-gt74>
- Ohminato T, Chouet BA, Dawson P, Kedar S (1998) Waveform inversion of very long period impulsive signals associated with magmatic injection beneath Kilauea Volcano Hawaii. *J Geophys Res* 103:23–839
- Poli P, Shapiro NM (2022) Rapid characterization of large volcanic eruptions: measuring the impulse of the Hunga Tonga Ha'apai explosion from teleseismic waves. *Geophys Res Lett*. <https://doi.org/10.1029/2022GL098123>
- Sakai S, Yamada T, Ide S, Mochizuki M, Shiobara H, Urabe T, Hirata N, Shinohara M, Kanazawa T, Nishizawa A, Fujie G, Mikada H (2001) Magma migration from the point of view of seismic activity in the volcanism of Miyake-Jima Island in 2000. *J Geogr* 110:145–155
- Saurel JM, Jacques E, Aiken C, Lemoine A, Retailleau L, Lavayssi'ere A, et al (2022) Mayotte seismic crisis: building knowledge in near real-time by combining land and ocean-bottom seismometers, first results. *Geophys J Int* 228:1281–1293. <https://doi.org/10.1093/gji/ggab392>
- Shinohara M, Yamada T, Akuhara T, Mochizuki K, Sakai S (2022) Performance of seismic observation by distributed acoustic sensing technology using a seafloor cable off Sanriku, Japan. *Front Mar Sci* 9:844506. <https://doi.org/10.3389/fmars.2022.844506>
- Sladen A, Rivet D, Ampuero JP, Barros LD, Hello Y, Calbris G, Lamare P (2019) Distributed sensing of earthquakes and ocean–solid earth interactions on seafloor telecom cables. *Nat Comm* 10:5777. <https://doi.org/10.1038/s41467-019-13793-z>
- Tarumi K, Yoshizawa K (2023) Eruption sequence of the 2022 Hunga Tonga–Hunga Ha'apai explosion from back-projection of teleseismic P waves. *Earth Planet Sci Lett* 602:117966. <https://doi.org/10.1016/j.epsl.2022.117966>
- Thurin J, Tape C, Modrak R (2022) Multi-event explosive seismic source for the 2022 Mw 6.3 Hunga Tonga submarine volcanic eruption. *Seism Record* 2:217–226. <https://doi.org/10.1785/0320220027>
- Tonga Cable Ltd. (2022) Torn apart missing 110 km domestic fibre optic cable may take year to replace. <https://www.tongacable.to/2022/03/02/torn-apart-missing-110km-domestic-fibre-optic-cable-may-take-year-to-replace/>. Accessed 28 Oct 2022
- Trnkoczy A (2012) Understanding and parameter setting of STA/LTA trigger algorithm, in *New Manual of Seismological Observatory Practice 2 (NMSOP-2)* IS 8.1. <http://nmsop.gfz-potsdam.de>. Accessed 29 May 2023
- Ugalde A, Becerril C, Villaseñor A, Ranero CR, Fernández-Ruiz MR, Martín-López S, González-Herráez M, Martins HF (2021) Noise levels and signals observed on submarine fibers in the canary Islands using DAS. *Seismol Res Lett* 93:351–363. <https://doi.org/10.1785/0220210049>
- Umakoshi K, Shimizu H, Matsuwo N (2001) Volcano-tectonic seismicity at Unzen Volcano, Japan, 1985–1999. *J Volcanol Geotherm Res* 112:117–131
- Wang HF, Zeng X, Miller DE, Fratta D, Feigl KL, Thurber CH, Mellors RJ (2018) Ground motion response to an ML 4.3 earthquake using co-located distributed acoustic sensing and seismometer arrays. *Geophys J Int* 213:2020–2036. <https://doi.org/10.1093/gji/ggy102>
- Watanabe H (1971) Determination of earthquake magnitude at regional distance in and near Japan. *Zisin1* 24:189–200
- Wessel P, Smith WHF (1998) New, improved version of generic mapping tools released. *Eos* 79:579
- Williams EF, Fernández-Ruiz MR, Magalhaes R, Vanhillo R, Zhan Z, González-Herráez M, Martins HF (2019) Distributed sensing of microseisms and teleseisms with submarine dark fibers. *Nat Comm* 10:5778. <https://doi.org/10.1038/s41467-019-13262-7>
- Williams EF, Zhan Z, Martins HF, Fernández-Ruiz MR, Martín-López S, González-Herráez M, Callies J (2022) Surface gravity wave interferometry and ocean current monitoring with ocean-bottom DAS. *J Geophys Res*. <https://doi.org/10.1029/2021JC018375>
- Withers M, Aster R, Young C, Beiriger J, Harris M, Moore S, Trujillo J (1998) A comparison of select trigger algorithms for automated global seismic phase and event detection. *Bull Seism Soc Am* 88:95–106
- Wright CJ, Hindley NP, Alexander MJ, Barlow M, Hoffmann L, Mitchell CN et al (2022) Surface-to-space atmospheric waves from Hunga Tonga–Hunga Ha'apai eruption. *Nature* 609:741–746. <https://doi.org/10.1038/s41586-022-05012-5>
- Yuen DA, Scruggs MA, Spera FJ, Zheng Y, Hu H, McNutt SR et al (2022) Under the surface: pressure-induced planetary-scale waves, volcanic lightning, and gaseous clouds caused by the submarine eruption of Hunga Tonga–Hunga Ha'apai volcano. *Earthq Res Adv* 2:100134. <https://doi.org/10.1016/j.eqrea.2022.100134>
- Yukutake Y, Ito H, Honda R, Harada M, Tanada T, Yoshida A (2011) Fluid-induced swarm earthquake sequence revealed by precisely determined

- hypocenters and focal mechanisms in the 2009 activity at Hakone volcano, Japan. *J Geophys Res* 116:B04308. <https://doi.org/10.1029/2010JB008036>
- Yukutake Y, Abe Y, Doke R (2019) Deep low-frequency earthquakes beneath the Hakone volcano, central Japan, and their relation to volcanic activity. *Geophys Res Lett* 46:11035–11043. <https://doi.org/10.1029/2019GL084357>
- Zhan Z (2019) Distributed acoustic sensing turns fiber-optic cables into sensitive seismic antennas. *Seismol Res Lett* 91:1–15. <https://doi.org/10.1785/0220190112>
- Zheng Y, Hu H, Spera FJ, Scruggs M, Thompson G, Jin Y et al (2023) Episodic magma hammers for the 15 January 2022 cataclysmic eruption of Hunga Tonga-Hunga Ha'apai. *Geophys Res Lett*. <https://doi.org/10.1029/2023GL102763>
- Zhu W, Beroza GC (2019) PhaseNet: a deep-neural-network-based seismic arrival-time picking method. *Geophys J Int* 216:261–273. <https://doi.org/10.1093/gji/ggy423>

Publisher's Note

Springer Nature remains neutral with regard to jurisdictional claims in published maps and institutional affiliations.

Daisuke Suetsugu Present position of DS: JICA volunteer for Tonga Geological Services